Applied Catalysis B: Environmental 232 (2018) 322–329

Contents lists available at ScienceDirect

Applied Catalysis B: Environmental

journal homepage: www.elsevier.com/locate/apcatb

Remarkably enhanced H_2 evolution activity of oxidized graphitic carbon nitride by an extremely facile K_2CO_3-activation approach

Jianjian Tian[a,b], Lingxia Zhang[a,*], Min Wang[a,b,c], Xixiong Jin[a,b], Yajun Zhou[c], Jianjun Liu[a], Jianlin Shi[a,*]

[a] State Key Laboratory of High Performance Ceramics and Superfine Microstructure, Shanghai Institute of Ceramics, Chinese Academy of Sciences, 1295 Dingxi Road, Shanghai 200050, PR China
[b] University of Chinese Academy of Sciences, No. 19A Yuquan Road, Beijing 100049, PR China
[c] School of Materials Science and Engineering, East China University of Science and Technology, 130 Meilong Road, Shanghai 200237, PR China

ARTICLE INFO

Keywords:
$g\text{-}C_3N_4$
Oxygen species
Photocatalysis
Hydrogen evolution
Visible light

ABSTRACT

The photocatalytic activity enhancement of graphitic carbon nitride ($g\text{-}C_3N_4$) in water splitting were commonly achieved by introducing various functional groups onto/into its planar structure. Herein, oxidized $g\text{-}C_3N_4$ (CNO) was prepared via an extremely facile K_2CO_3 activation approach. The high-resolution XPS spectra and solid-state ^{13}C NMR spectra confirmed the successful introduction of O-containing groups and O atoms were inherited the original molecular framework of $g\text{-}C_3N_4$, but exhibited effectively enlarged bonded with C atoms rather than N atoms in the tri-s-triazine structure of $g\text{-}C_3N_4$. CNO inherited the original molecular framework of $g\text{-}C_3N_4$, but exhibited effectively enlarged surface area and enhanced visible light absorption, and more attrractively, the band structure of $g\text{-}C_3N_4$ could be well-tuned with the introduction of oxygen species. Importantly, the surface O-containing moieties could strongly interact with cocatalyst Pt and thus remarkably promote interfacial electron transfer and consequent photo-generated charge carrier separation. Consequently, the as-obtained CNO exhibited the remarkably enhanced photocatalytic performance with a H_2 evolution rate of 199.7 μmol h^{-1}, which is 9 times that of $g\text{-}C_3N_4$ (22.2 μmol h^{-1}).

1. Introduction

Photocatalytic H_2 evolution is an environmentally friendly solution to directly capture and store solar energy [1], which has been pursued for decades since the first demonstration on photocatalytic water splitting by TiO_2 in 1972 [2]. However, because the solar-to-H_2 efficiency of photocatalytic water splitting is still very low, it is urgent to develop highly efficient visible-light-response photocatalysts. Metal-free graphitic carbon nitride ($g\text{-}C_3N_4$) with suitable band structure (normally $E_g = 2.7$ eV, $E_{CB} = -1.2$ eV and $E_{VB} = 1.5$ eV vs RHE) has attracted extensive interest in recent years. In particular, $g\text{-}C_3N_4$ can be easily synthesized by thermal polymerization of ordinary precursors (such as urea, melamine or dicyanamide etc.) and shows good thermal and chemical stability. Whereas, pristine $g\text{-}C_3N_4$ suffers from limited visible-light absorption, high recombination rate of photoexcited charge carriers and thus exhibits low photocatalytic activity and conversion efficiency. Various methods have been developed to address these problems, such as heteroatom doping [3–5], copolymer construction [6], low-dimensional nanostructure synthesis [7–9], crystal engineering [10], hetero-semiconductor or conductor coupling [11], etc.

It is well known that the water splitting takes place on the photocatalyst surface, so the doping of different functional groups on its surface may significantly alter the surface state without changing the performance of the photocatalyst. This triggers great enthusiasm of research to introduce a variety of functional groups into $g\text{-}C_3N_4$ network and it has been found the functional groups incorporated into $g\text{-}C_3N_4$ molecular can work wonders. These functional groups can be considered as functional defects and seemed to be the real active sites of photocatalytic reaction. We have post-grafted various aromatic heterocycles on the surface of $g\text{-}C_3N_4$ to expand the π-delocalized system, improve the charge transfer ability, and thus enhance the photocatalytic activity of $g\text{-}C_3N_4$ [12]. It was also reported that the isolated oligomers of melem with abundant peripheral functional groups were thermodynamically more reductive than the longer ones, and therefore could induce faster extraction of the photogenerated charges [13]. Other researchers found that the coordinated cyanamide moiety onto $g\text{-}C_3N_4$ could be regarded as photocatalytic relevant defect, which

* Corresponding authors.
E-mail addresses: Zhlingxia@mail.sic.ac.cn (L. Zhang), jlshi@mail.sic.ac.cn (J. Shi).

https://doi.org/10.1016/j.apcatb.2018.03.076
Received 5 December 2017; Received in revised form 7 March 2018; Accepted 21 March 2018
Available online 23 March 2018
0926-3373/

promoted the interactions between co-catalyst and g-C_3N_4, and facilitated interfacial electron separation [14]. B. Lotsch et al also found that the inserted urea moiety was the preferential docking site for co-catalyst Pt, thus leading to the improved intrinsic photocatalytic performance [15]. From these reports, we can see that the functional groups, which were considered previously as the "defects", seem to be the real active sites in g-C_3N_4 for photocatalysis. The above-mentioned functional groups such as amino groups, cyanamide moiety and urea are actually the intrinsic components or structure ligands of g-C_3N_4. As a result, a critical question remains: what is the role of suspending/dangling bonds in photocatalytic H_2 evolution, if deliberately introduced? Considering O-containing groups are hydrophilic and the electronegativity of oxygen is largely different from the elements (C, N, H) of g-C_3N_4, here we choose O-containing groups as the guest units for creating suspending/dangling bonds on pristine g-C_3N_4.

Bandosz et al introduced O-containing groups (C═O, N−O, OH) into g-C_3N_4 nanolayers and exfoliated g-C_3N_4 by Hummers method to increase the chemical heterogeneity and polarity of g-C_3N_4 [16]. Sungjin Park et al synthesized oxidized g-C_3N_4 to improve its hydrophility by treating g-C_3N_4 with $KMnO_4$ in the presence of sulfuric acid [17]. Xie et al obtained oxidized g-C_3N_4 through HNO_3/H_2SO_4 treatment of pristine g-C_3N_4 and enhanced the singlet O generation in g-C_3N_4 [18]. And also there are other ways to introduce O-containing groups into g-C_3N_4, such as successively thermal oxidation [19], hydrothermal treatment in NaOH solution [20], etc. However, most of these methods are complicated, and some are even violent or dangerous.

Here in this work, we successfully developed an extremely facile K_2CO_3 activation strategy to fabricate oxidized g-C_3N_4 (CNO). Oxygen atoms have been bonded to C atoms of tri-s-triazine during the oxidation process. Compared with the pristine g-C_3N_4, the as-obtained CNO photocatalysts showed enlarged specific surface area, improved optical absorption ability and promoted interfacial charge transfer. With the increase of activation temperature, the conductive potential of CNO continuously declined while its valence band potential changed slightly, thus the band structure of CNO can be well tuned. Very encouragingly, the photocatalytic H_2 evolution performance by water-splitting under visible light has been remarkably enhanced by 9 times by such a facile approach.

2. Experimental section

2.1. Sample preparation

Preparation of g-C_3N_4: Sample g-C_3N_4 was prepared by thermally decomposing urea at 550 °C in an alumina crucible with a cover for 2 h in static air with a ramp rate of 5 °C min^{-1}. Then, the crucible was cooled to room temperature naturally. The resultant yellow product was collected and ground into fine powder for further use and was denoted as CN.

Preparation of oxidized g-C_3N_4: The CNO samples were prepared via K_2CO_3 activation treatment of pristine CN. Briefly, 1 g as-prepared CN powder was added to the well-dissolved aqueous K_2CO_3 solution (0.1 g K_2CO_3 in 80 mL H_2O), and the resulting mixture was stirred for 8 h at room temperature. Then the solution was centrifugal washed with water five times and freeze dried overnight. The solid power was put into a ceramic boat, which was placed at the middle of a horizontal quartz tube furnace and heated at a certain temperature for 2 h in Ar atmosphere. The product was denoted as CNO-*x*, in which *x* represents the temperature of K_2CO_3 activation treatment.

2.2. Characterization

Characterizations: Elemental analysis (C, H, N) was performed on a Vario EL microanalyzer. The BET surface area was measured on a Micromeritics Tristar 3000 system. The energy dispersive X-ray spectrum (EDS) obtained from an attached Oxford Link ISIS energy-dispersive spectrometer fixed on a JEM-2010 electron microscope. X-ray diffraction (XRD) measurement was conducted on a Rigaku D/Max 2200PC diff ;ractometer (Cu Kα radiation). Fourier transformed infrared (FT-IR) spectra was recorded with a Nicolet iS10 FTIR spectrometer. Solid-state ^{13}C NMR spectra was performed using a Bruker Advance III 600spectrometer. X-ray photoelectron spectroscopy (XPS) measurement was carried out on a Thermo Scientic Escalab 250 spectrometer with Al Kα radiation as the excitation source. The UV–vis absorption spectra was recorded in the range of 300–800 nm with a UV-3600 PC Shimadzu spectroscope using $BaSO_4$ as a reference. Photoluminescence spectra (PL) of the samples were obtained at room temperature excited by incident light of 380 nm using a fluorescence spectrometer (Shimadzu RF-5301PC).

Electrochemical Analysis: Electrochemical measurement was conducted on a CHI 760E electrochemical workstation (Chenhua Instruments, Shanghai, China) with a standard three-electrode cell, which employed an FTO electrode deposited with the obtained sample as working electrode, a platinum sheet as counter electrode and saturated Ag/AgCl as reference electrode. A 300 W Xe lamp (PLS-SEX300C, Perfectlight Limited, Beijing) with a 420 nm cut-off filter was used as visible light source. The working electrode was prepared by electrophoretic deposition in an acetone solution (25 mL) containing sample powder (20 mg) and iodine (40 mg). The FTO glass was kept in the above solution for 5 min with a 10 V bias under potentiostat control. After being calcined for 2 h in an oven at 150 °C, a homogeneous film was obtained. 50 mL of 0.2 M Na_2SO_4 was used as electrolyte solution, which represented the best compromise between activity and stability of the sample.

Photocatalytic hydrogen evolution test: The visible light-induced H_2 evolution was carried out in a Pyrex top-irradiation reaction vessel connected to a closed glass gas-circulation system (Lab-Solar-III AG, Perfectlight Limited, Beijing). A 300 W xenon lamp (CEL-HXF300, Ceaulight, Beijing) with a 420 nm cut-off filter was chosen as a visible light source, and the light intensity was 230 mW cm^{-2} (tested by FieldMaxII-TO, Coherent). Photocatalyst (100 mg) was suspended in an aqueous solution (100 mL) containing triethanolamine (10 vol %), and 3 wt % Pt was loaded on the surface of the catalyst by in-situ photodeposition using H_2PtCl_6 as the precursor. The reactant solution was evacuated several times to remove air prior to the irradiation experiment. The temperature of the reaction solution was maintained at 10 °C by a flow of cooling water during the photocatalytic reaction. The evolved gas was analyzed by gas chromatography (GC7900, Techcomp) equipped with a thermal conductive detector (TCD) and a 5 Å molecular sieve column, using N_2 as carrier gas.

3. Results and discussion

As can be seen from the results of elemental analysis shown in Table 1, O contents in all CNO-*x* samples are twice higher than that in pristine CN, which gradually increase at the elevated activation temperatures. Besides, the C/N molar ratio increases from 0.69 of the pristine CN to 0.74 of CNO-650. The contents of N and H decrease significantly after the K_2CO_3 treatment. These reveal that oxygen species have been successfully introduced onto/into the framework of g-C_3N_4. And EDS spectrum (Fig. S1) shows that the atomic percentage of K in CNO-550 is just 0.09%, so the remained K atom on the surface of g-C_3N_4 can be ignored. The terminal $-NH_2$ groups, remained after the incomplete polymerization of urea during g-C_3N_4 formation, seem to be the most possible targets of K_2CO_3 attack during the oxygen species introduction and g-C_3N_4 activation. These oxygen species were further characterized by solid-state ^{13}C NMR spectra and XPS analysis as discussed below. The specific surface area (BET) of CNO gently increases with the increasing activation temperature. The CNO-650 sample shows a maximum specific surface area of 132.40 $m^2 g^{-1}$, remarkably higher than that of CN (67.48 $m^2 g^{-1}$), which enables the exposure of more

Table 1
Bulk contents of C, N, and H by elemental analysis, BET surface areas and band structures of CN and CNO-*x* samples.

Sample	C wt%	N wt%	H wt%	O wt%	C/N atomic ratio	BET $m^2 g^{-1}$	E_g (eV)	CB (V)
CN	35.08	59.16	1.73	4.03	0.69	67	2.69	−1.07
CNO-500	34.75	55.10	1.66	8.49	0.74	84	2.65	−1.03
CNO-550	34.79	54.96	1.66	8.59	0.74	94	2.53	−0.91
CNO-600	34.75	54.78	1.69	8.78	0.74	101	2.46	−0.84
CNO-650	34.81	54.68	1.41	9.10	0.74	132	2.38	−0.76

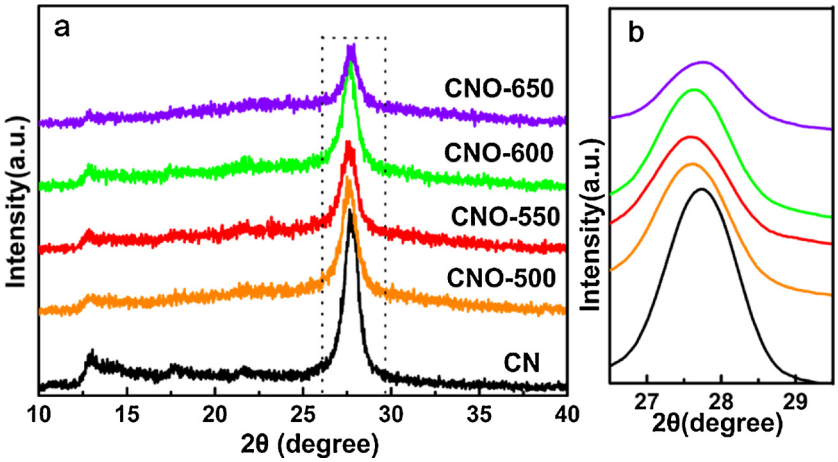

Fig. 1. XRD patterns of (a) the pristine CN and CNO-*x* samples and (b) magnified view of the main peak at around 27.7°.

catalytic active sites for adsorption and surface reaction [21].

The chemical structures of all samples were characterized by X-ray diffraction (XRD) patterns and FT-IR spectroscopy. As shown in Figs. 1 and 2a, the XRD patterns and FT-IR spectra of CNO-*x* are similar to that of pristine CN, confirming that the molecular framework of g-C_3N_4 has been well preserved. All the samples exhibit two distinct diffraction peaks, the stronger one at around 27.79° represents the (002) interlayer reflection of the graphitic-like structure, while the other weaker reflection at about 13.0° is attributed to the (100) in-plane repeated units of tri-s-triazine [22]. Clearly, the (002) peak down-shifts from 27.79° (CN) to 27.62° (CNO-550) at the gradually increased activation temperature, corresponding to the increase of the inter-planar distance from 0.320 nm of CN to 0.323 nm of CNO-550, and in the meantime, the (002) peak up-shifts from 27.62° (CNO-600) to 27.88° (CNO-650) due to the further increase of activation temperature beyond 600 °C. Besides, the diffraction peaks of CNO-*x* samples are weakened and broadened in comparison with those of the pristine CN, indicating the loss of ordered structures to a certain level after K_2CO_3 activation. This disruption of g-C_3N_4 structure could help separate electron and hole to varied extents [23]. Fig. 2a shows the FT-IR spectra of CN and CNO-*x* samples. The intense peak at ca. 812 cm^{-1} is typical of the out-of-plane deformation vibration modes of triazine units [24]. The multiple bands between 1200 and 1650 cm^{-1} correspond to the stretching modes of aromatic C/N heterocycle [25]. The broad peaks at around 3100–3400 cm^{-1} can be assigned to stretching vibration modes of the $-NH_2$ group and −OH group of the adsorbed H_2O from air. In addition, a new band at 2180 cm^{-1} assigned to vibrations of C≡N appeared in CNO-*x* can be attributed to the fracture and restructure of C−N bonds in the tri-s-triazine ring during K_2CO_3 activation [16]. Researchers have reported that it is difficult to discriminate O-containing species in the FT-IR spectra, because the vibrations by these O-containing moieties could be covered by strong aromatic C−N stretching in CN [26,27]. So we took further more characterizations to identify the chemical environment of oxygen species.

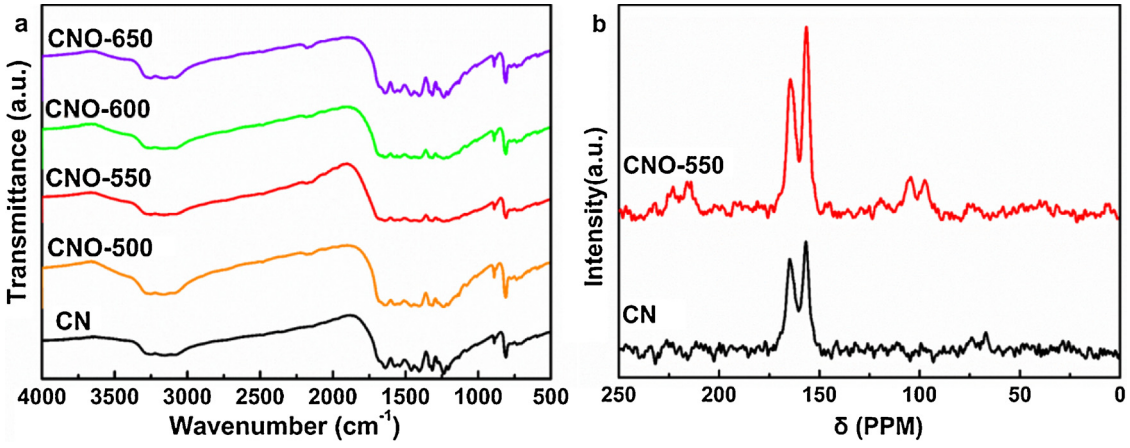

Fig. 2. (a) FT-IR spectra of all samples and (b) The solid-state ^{13}C NMR spectra of CN and CNO-550 samples.

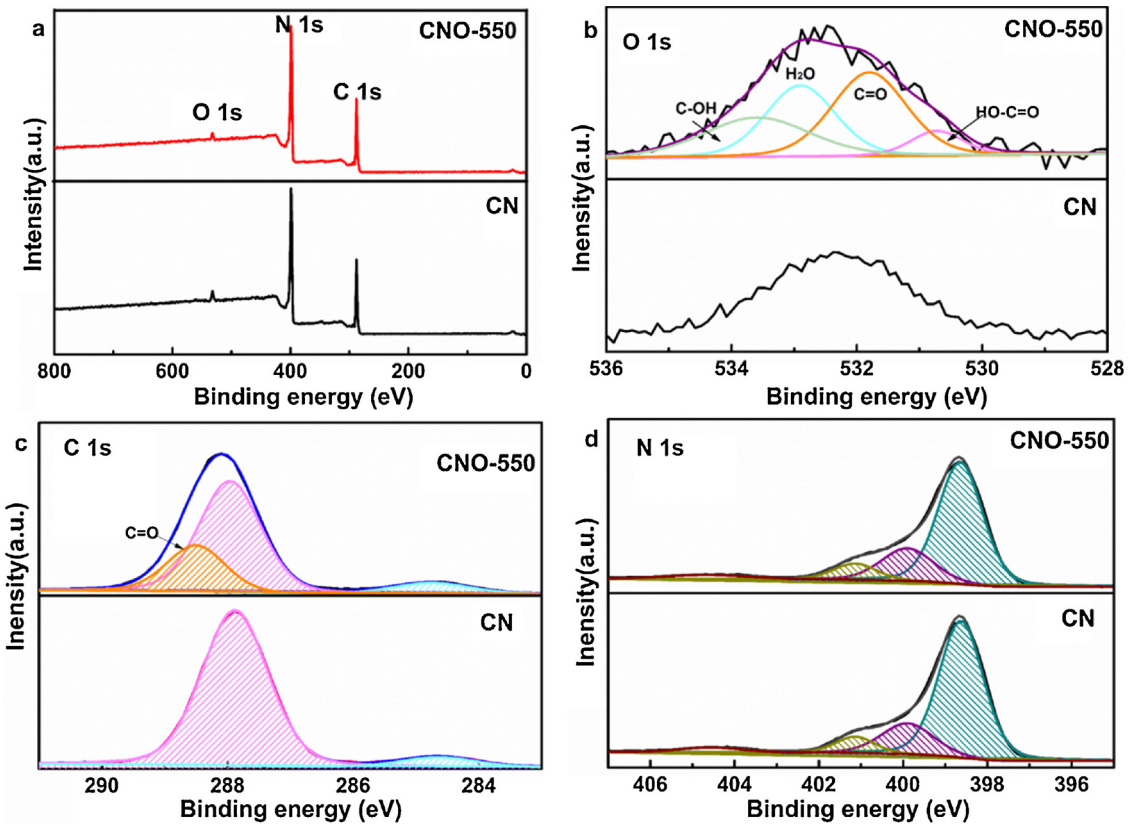

Fig. 3. (a) XPS survey spectra and high-resolution O 1s (b), C 1s (c), N 1s (d) XPS spectra of CN and CNO-550 samples.

The solid-state ^{13}C NMR spectra of CN and CNO-550 are presented in Fig. 2b. Both samples show two strong peaks at 156.5 and 165.1 ppm corresponding to the chemical shifts of C_3N and C_2N-NH_x in the heptazine units, respectively [6]. CNO-550 exhibits several extra peaks at 214.3 and 222.0 ppm, which can be ascribed to the contributions by carbonyl/carboxyl carbons (usually located at 165–240 ppm) [28]. The peaks at 100–120 ppm is attributed to unsaturated C originated from the disruption of g-C_3N_4 structure. Thus, based on the ^{13}C NMR results, we can conclude that during the K_2CO_3 activation, partial C—N bonds are broken and oxygen species are introduced and bonded to carbon, forming carbonyl/carboxyl species in the melon skeleton structure of g-C_3N_4. This is also confirmed by the analysis of X-ray photoelectron spectroscopy (XPS).

The XPS spectra of CN and CNO-550 were further collected to check the change of surface elemental composition and chemical states. It can be clearly seen from the XPS survey spectra (Fig. 3a) that only C, N and O elements are present in CN and CNO-550. The high-resolution O 1s signals (Fig. 3b) of these two samples show that the intensity of O 1s peak of CNO-550 is much stronger than that of pristine CN, which is in accordance with the results of elemental analysis. The small amount of O in CN can be attributed to the atmospheric water adsorbed on the surface. Comparatively, there are several O-containing groups such as HO—C=O (530.7 eV), C=O (531.8 eV) and C—OH (533.4 eV) in CNO-550 [27,29]. The peak at binding energy of 532.9 eV is attributed to the surface adsorbed water [30]. The presences of these carbon and oxygen species confirm that O atoms are bonded to C atoms in the molecular framework of g-C_3N_4 in CNO-*x*. These polar functional moieties will result in increased hydrophilicity and photocatalytic activity. The C 1s XPS spectra of both CN and CNO-550 contain two peaks centered at 284.6 and 287.9 eV, corresponding to the aromatic C atoms and the sp^2 hybridized C atoms in the heptazine units, respectively [31]. It is worth noting that the peak-area at 287.9 eV of CNO-550 is lower than that of CN, and there is a new C=O peak at 288.5 eV in the C 1s XPS spectrum of CNO-550 [17], further evidencing that O atoms are bonded to C atoms rather than N atoms in tri-s-triazine of g-C_3N_4 after K_2CO_3 activation, which is in accordance with the significant decrease of N content and the increase of O content as evidenced by elemental analysis. As shown in Fig. 3d, the high-resolution N 1s spectra can be deconvoluted into three components at about 398.6, 399.9 and 401.1eV, corresponding to sp^2 hybridized nitrogen (C—N=C, N_2C), tertiary nitrogen groups (N—$(C)_3$, N_3C) and amino groups (C—NH_x, N_1C) in the heptazine substructures, respectively [32]. Further analysis of the N 1s XPS reveals that the peak-area of N_2C decreases from 72.97% of CN to 69.38% of CNO-550, while that of N_1C increases from 7.65% of CN to 8.91% of CNO-550, indicating the slight loss of tri-s-triazine in g-C_3N_4 after K_2CO_3 activation.

According to the above results, we propose the possible existing forms of O atoms in the framework of g-C_3N_4, as illustrated in Scheme 1. The mechanism of K_2CO_3 activation is proposed to be that K^+ could intercalate into the CN layers, which makes the tri-s-triazine structure distorted and the interlayer distance expanded to certain extents [33]. Then O atoms bond with C atoms in the tri-s-triazine units at elevated temperatures. These surface O-containing bonds on the basal plane of g-C_3N_4 could enhance the hydrophilicity of the photocatalyst and may work as active sites because of their strong electron withdrawing capability.

The photocatalytic activities of the CN and CNO-*x* were evaluated using H_2 evolution rate under visible light irradiation ($\lambda > 420$ nm). As shown in Fig. 4a, all the CNO-*x* samples present significantly enhanced H_2 production rate compared to CN. Apparently, the results suggest that there should be an optimum O concentration in CNO-*x* for achieving the maximized photocatalytic H_2 evolution rate. Among the samples prepared, CNO-550 exhibits the best photocatalytic performance with a H_2 evolution rate of 199.7 μmol h^{-1}, which is 9 times that of CN (22.2 μmol h^{-1}).

The stability of CNO-550 has also been charactrerized by repeating

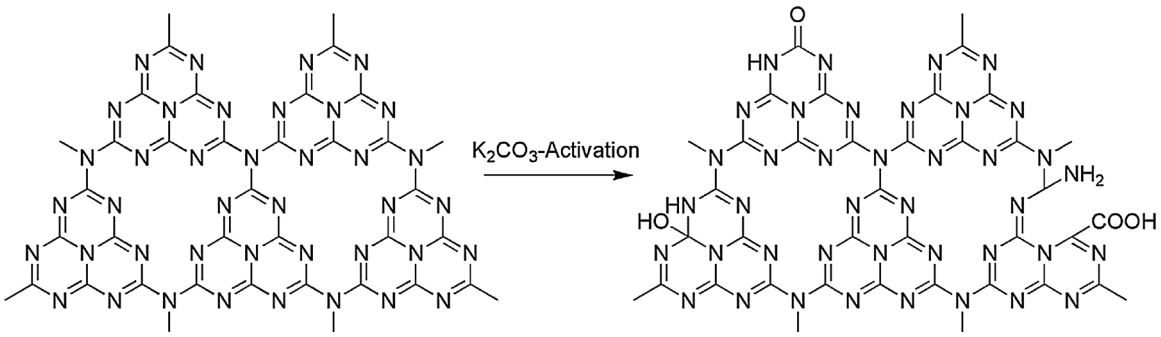

Scheme 1. Illustration of the possible existing form of O atoms in the framework of g-C_3N_4.

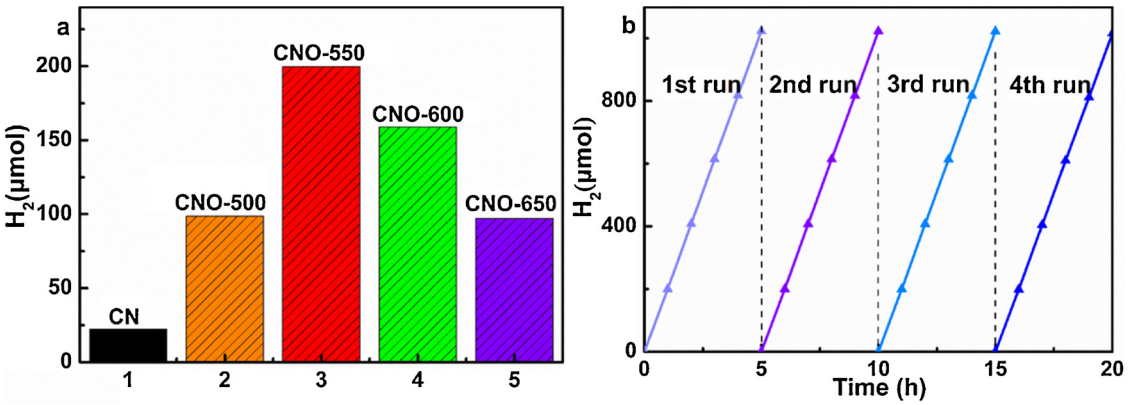

Fig. 4. (a) H_2 evolution rates on CN and CNO-*x*, (b) Cycling stability tests of H_2 evolution on CNO-550.

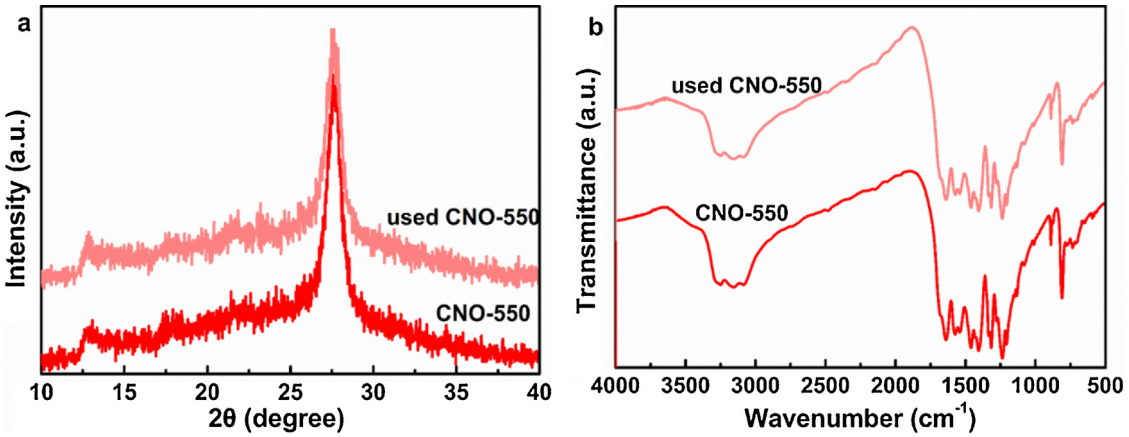

Fig. 5. (a) XRD patterns and (b) FT-IR spectra of CNO-550 and used CNO-550 samples.

the photocatalytic experiments under the same conditions for four cycles (20 h) (Fig. 4b). Clearly, there is no significant decrease in the H_2 evolution rate after four consecutive cycles. After photocatalytic reaction, the used CNO-550 sample was collected by centrifugation. Fig. 5 compares the XRD patterns and FT-IR spectra of CNO-550 sample before (CNO-550) and after (used CNO-550) the photocatalytic reaction. It can be found that, there are no noticeable alternations in the crystal and chemical structures, suggesting the excellent reusability and stability of this photocatalyst.

There are several crucial parameters helping to achieve the maximized photocatalytic activity of semiconductors including surface area, hydrophilicity, light absorption, band structure, separation of charge carriers, etc [34]. The roles and effects of these factors on H_2 evolution rates of the as-synthesized samples are discussed as follows. As mentioned above, enlarged specific surface area could result in more catalytic active sites being exposed. Table 1 displays that the surface area of CNO-*x* gently increases with the increasing activation temperature. The CNO-650 sample shows a maximum specific surface area, but its H_2 evolution rate is not the highest, indicating that enlarged specific surface area is not the dominant contributor in promoting the photocatalytic activity of g-C_3N_4. Considering there is only a small amount of hydrophilic groups (O atomic content: 0.54%, Fig. S1) introduced into g-C_3N_4, the surface hydrophilicity of g-C_3N_4 has been inproved a little but not significantly. Therefore, we believe that the improved surface hydrophilicity cannot play the key role in enhancing the photocatalytic activity of g-C_3N_4.

The optical absorptions of CN and CNO-*x* samples were characterized using UV–vis absorption spectra. As shown in Fig. 6, O-bonding into tri-s-triazine structure of g-C_3N_4 dramatically improves their optical absorption properties. A progressive redshift of the absorption edge has been achieved with the increase of O content, indicating that the enhanced visible light harvesting of the photocatalyst, and

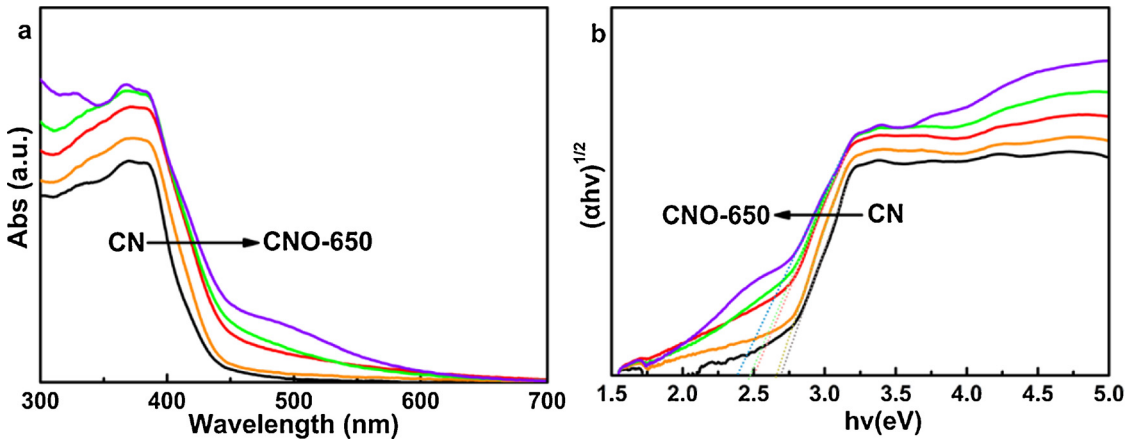

Fig. 6. (a) UV–vis absorption spectra and (b) Plots of transformed Kubelka–Munk function versus photon energy of as-synthesized samples.

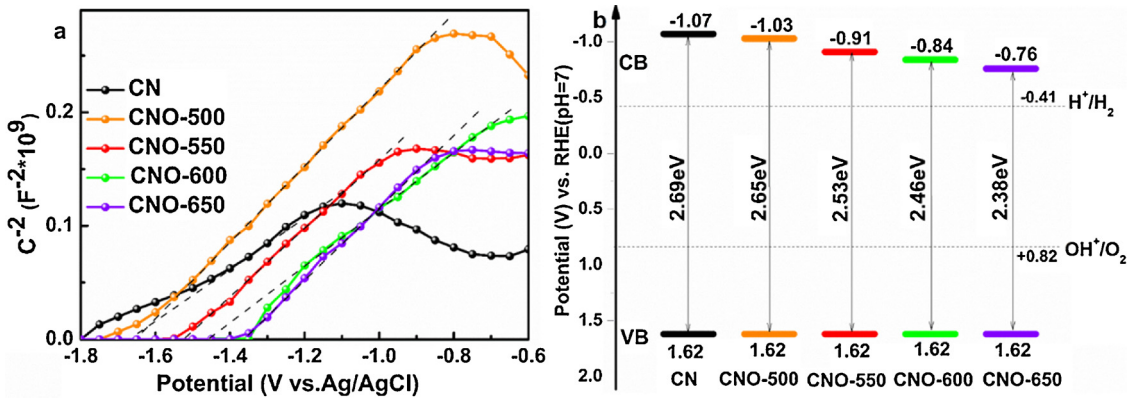

Fig. 7. (a) Mott–Schottky plots and (b) Band structure alignments for pristine CN and CNO-*x*.

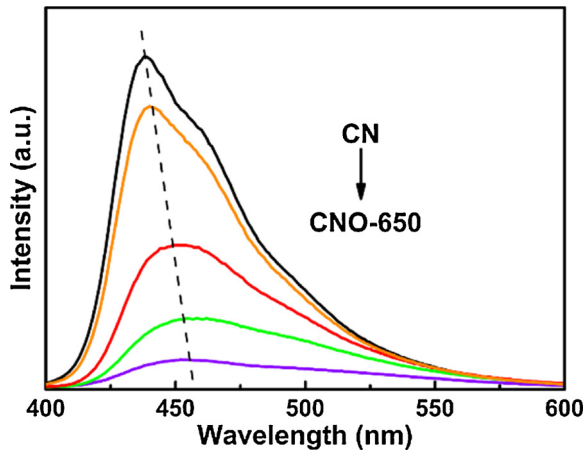

Fig. 8. PL spectra (excitation wavelength: 380 nm) of as-synthesized samples.

subsequently elevated photocatalytic activity of g-C_3N_4 [19]. In the UV–vis absorption spectra of the samples, the absorption edge near 400 nm is attributed to π–π* transitions in g-C_3N_4 conjugated structure [35], while the additional long wavelength absorption is assigned to the defect-related state below CBM of g-C_3N_4 after O bonding with C. Fig. 6b exhibits the plots of transformed Kubelka–Munk functions of all samples, which determine the bandgaps as listed in Table 1. E_g value decreases from 2.69 eV of CN to 2.38 eV of CNO-650, implying that the electronic structure of g-C_3N_4 has been substantially modified. The narrowed band gap not only helps to enhance the absorption of the visible light but also benefits overcoming the thermodynamic barrier of the water splitting reaction [36].

To dive into more details of band structure, Mott – Schottky (MS) tests were carried out. Fig. 7a shows typical MS plots of CN and CNO-*x* in dark, which reveals the n-type characteristics of all samples according to the positive slope of the linear plots [4]. The measured potentials can be converted to the reversible hydrogen electrode (RHE) scale via the Nernst equation:

$$E_{RHE} = E_{Ag/Cl} + 0.05916pH + E^0_{Ag/Cl}$$

where E_{RHE} is the converted potential vs. RHE, $E_{Ag/AgCl}$ is the experimental potential measured against the Ag/AgCl reference electrode, and $E^\circ_{Ag/AgCl}$ is the standard potential of Ag/AgCl at 298 K (0.1976 V) [37]. The calculated conduction band edges of all samples are listed in Table 1. In comparison with CN, a gradual downshift of the conduction band edge of CNO-*x* could be observed. Combined with the above results of bandgaps, the CB (conduction band) edges and VB (valence band) edges of CN and CNO-*x* could be calculated, and their band alignments are shown in Fig. 7b. And the calculated valence band edges are consistent with the result of valence band XPS spectra (shown in Fig. S2). It is obvious that all the samples have suitable CB and VB positions to reduce H_2O to H_2. The data suggests that the CB position gradually declines while VB position changes little by the introduction of O atoms into g-C_3N_4. This is in accordance with the previous report that the conduction band minimum (CBM) and the valence band maximum (VBM) of g-C_3N_4 are composed predominantly of Cp_z and Np_z orbitals [38]. As O atom is much more electronegative than N atom, therefore O atom would be more preferrable in bonding with C by withdrawing electrons from the nearest C atoms than N atom, leading to the delocalized electron distribution in g-C_3N_4 network. Subsequently, a defect-related state below CBM of g-C_3N_4 can be

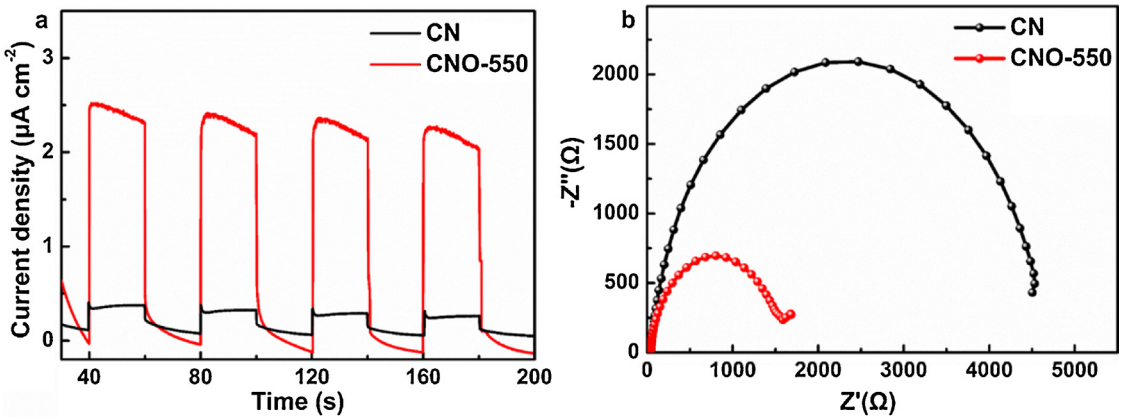

Fig. 9. (a) Transient photocurrents under cycling illuminations and (b) EIS Nyquist plots in dark of CN and CNO-550.

formed. This defect-related state is the origin of the Urbach tail in the optical absorption spectra of CNO-*x* in Fig. 6a.

The hybridized band edges associated with surface O-containing bonds could well facilitate electron donation from g-C_3N_4 to the cocatalyst Pt nanoparticles by so-called metal-support interaction (MSI) [39]. According to the recent findings based on experimental and computational investigations by Bettina V. Lotsch's group, O moieties are much stronger in interaction with Pt than other elements in the materials, which facilitates the transfer of photogenerated electrons to hydrogen evolving centers of Pt cocatalyst [14,15]. On the other hand, O bonding with C benefites the transition of photogenerated electrons from VB to CB, because of the high electron-withdrawing ability of oxygen moieties, resembling the role of built-in electric field in semiconductors [40]. The promoted interfacial charge transfer in activated samples was also verified by photoluminescence and electrochemical analysis. Studies on the photochemical reduction of H_2O to H_2 suggest that the lower CB position of photocatalyst accords with the weaker reduction capability of the photo-induced electrons [12], which explains why CNO-650 did not demonstrate the highest H_2 evolution rate though having the largest surface area and the strongest light absorption.

Fig. 8 reveals the photoluminescence curves (PL) of CN and CNO-*x* at an excitation wavelength of 380 nm. The emission peaks of CNO-*x* shift toward longer wavelength compared to that of CN, which is in agreement with the narrowed bandgap of CNO-*x*. In the meantime, the PL emission intensity of CNO-*x* gradually decreases as the O content increases, this indicates that the bonded O atoms on the tri-s-triazine structure of g-C_3N_4 has effectively prevented photogenerated charge carriers from recombination [41]. Moreover, the enhanced photocurrent response as well as the smaller impedance arc radius of CNO-550 (shown in Fig. 9), verifys the prohibited recombination and promoted interfacial charge transfer of photo-generated electron–hole in CNO-550 in comparison with the pristine CN [42].

4. Conclusions

Here in this work, we have successfully developed oxidized graphitic carbon nitride (CNO) via an extremely facile K_2CO_3 activation approach. Oxygen species were successful introduced into g-C_3N_4 and O atoms were bonded to C atoms in tri-s-triazine of g-C_3N_4 to form C═O, HO−C═O, C−OH groups. The conduction band position become lowered while the valence band position remains almost unaffected by introducing increased amount of oxygen species into g-C_3N_4, thus the band structure of CNO can be conveniently tuned. The oxidation treatment by K_2CO_3 activation does not damage the original framework of g-C_3N_4, but effectively enlarges its surface area and enhances the visible light absorption. More importantly, the surface O-containing bonds created by K_2CO_3 activation would strongly interact with the loaded Pt cocatalyst, thus promoting the photo-excited electron transfer and separation of charge carriers. As a result, the obtained CNO exhibits significantly enhanced visible-light photocatalytic activity in H_2 evolution over the pristine g-C_3N_4. This work provides an extremely facile strategy to introduce oxygen species into g-C_3N_4, which creates a novel high-performance g-C_3N_4 photocatalyst with tunable band structure.

Acknowledgements

We acknowledge financial supports from the National Key Basic Research Program of China (2013CB933200). We thank Jiangsu National Synergetic Innovation Center for Advanced Materials (SICAM).

Appendix A. Supplementary data

Supplementary material related to this article can be found, in the online version, at doi:https://doi.org/10.1016/j.apcatb.2018.03.076.

References

[1] Y. Li, H. Xu, S. Ouyang, D. Lu, X. Wang, D. Wang, J. Ye, Surface alkalinized g-C_3N_4 toward enhancement of photocatalytic H_2evolution under visible-light irradiation, J. Mater. Chem. A 8 (2016) 2943–2950.
[2] A. Fujishima, K. Honda, Electrochemical photolysis of water at a semiconductor electrode, Nature 238 (1972) 37.
[3] G. Liu, P. Niu, C. Sun, S.C. Smith, Z. Chen, G. Lu, H. Cheng, Unique electronic structure induced high photoreactivity of sulfur-doped graphitic C_3N_4, J. Am. Chem. Soc. 132 (2010) 11642–11648.
[4] Q. Ruan, W. Luo, J. Xie, Y. Wang, X. Liu, Z. Bai, C.J. Carmalt, J. Tang, A nano-junction polymer photoelectrode for efficient charge transport and separation, Angew. Chem. Int. Ed. 129 (2017) 8333–8337.
[5] Y. Zhou, L. Zhang, J. Liu, X. Fan, B. Wang, M. Wang, W. Ren, J. Wang, M. Li, J. Shi, Brand new P-doped g-C_3N_4: enhanced photocatalytic activity for H_2 evolution and rhodamine B degradation under visible light, J. Mater. Chem. A 3 (2015) 3862–3867.
[6] X. Fan, L. Zhang, M. Wang, W. Huang, Y. Zhou, M. Li, R. Cheng, J. Shi, Constructing carbon-nitride-based copolymers via Schiff base chemistry for visible-light photocatalytic hydrogen evolution, Appl. Catal. B: Environ. 182 (2016) 68–73.
[7] X. Zhang, X. Xie, H. Wang, J. Zhang, B. Pan, Y. Xie, Enhanced photoresponsive ultrathin graphitic-phase C_3N_4 nanosheets for bioimaging, J. Am. Chem. Soc. 135 (2013) 18–21.
[8] X. Zhang, H. Wang, H. Wang, Q. Zhang, J. Xie, Y. Tian, J. Wang, Y. Xie, Single-layered graphitic-C_3N_4 quantum dots for two-photon fluorescence imaging of cellular nucleus, Adv. Mater. 26 (2014) 4438–4443.
[9] J. Xu, H. Wang, C. Zhang, X. Yang, S. Cao, J. Yu, M. Shalom, From millimeter to subnanometer: vapor–solid deposition of carbon nitride hierarchical nanostructures directed by supramolecular assembly, Angew. Chem. Int. Ed. 56 (2017) 8426–8430.
[10] J. Wang, Y. Shen, Y. Li, S. Liu, Y. Zhang, Crystallinity modulation of layered carbon nitride for enhanced photocatalytic activities, Chem. Eur. J. 22 (2016) 12449–12454.
[11] M. Ye, Z. Zhao, Z. Hu, L. Liu, H. Ji, Z. Shen, T. Ma, 0D/2D heterojunctions of vanadate quantum dots/graphitic carbon nitride nanosheets for enhanced visible-light-driven photocatalysis, Angew. Chem. Int. Ed. 56 (2017) 8407–8411.
[12] J. Tian, L. Zhang, X. Fan, Y. Zhou, M. Wang, R. Cheng, M. Li, X. Kan, X. Jin, Z. Liu, J. Shi, A post-grafting strategy to modify g-C_3N_4 with aromatic heterocycles for

enhanced photocatalytic activity, J. Mater. Chem. A 4 (2016) 13814–13821.
[13] W. Lau, M. Mesch, V. Duppel, V. Blum, J. Senker, V. Lotsch, Low-molecular-weight carbon nitrides for solar hydrogen evolution, J. Am. Chem. Soc. 137 (2015) 1064–1072.
[14] W. Lau, I. Moudrakovski, T. Botari, S. Weinberger, B. Mesch, V. Duppel, J. Senker, V. Blum, V. Lotsch, Rational design of carbon nitride photocatalysts by identification of cyanamide defects as catalytically relevant sites, Nat. Commun. 7 (2016) 12165.
[15] W. Lau, H. Yu, Z.W.F. Ehrat, T. Botari, I. Moudrakovski, T. Simon, V. Duppel, E. Medina, K. Stolarczyk, J. Feldmann, Urea-modified carbon nitrides: enhancing photocatalytic hydrogen evolution by rational defect engineering, Adv. Energy Mater. 7 (2017) 1602251.
[16] D. Giannakoudakis, N. Travlou, J. Secor, T. Bandosz, Oxidized g-C_3N_4 nanospheres as catalytically photoactive linkers in MOF/g-C_3N_4 composite of hierarchical pore structure, Small 13 (2017) 1601758.
[17] J. Oh, R. Yoo, S. Kim, Y. Lee, D. Kim, S. Park, Oxidized carbon nitrides: water-dispersible, atomically thin carbon nitride-based nanodots and their performances as bioimaging probes, Chemistry 21 (2015) 6241–6346.
[18] H. Wang, S. Jiang, S. Chen, D. Li, X. Zhang, W. Shao, X. Sun, J. Xie, Z. Zhao, Q. Zhang, Enhanced singlet oxygen generation in oxidized graphitic carbon nitride for organic synthesis, Adv. Mater. 28 (2016) 6940–6945.
[19] J. Fu, B. Zhu, C. Jiang, B. Cheng, W. You, J. Yu, Hierarchical porous O-doped g-C_3N_4 with enhanced photocatalytic CO_2 reduction activity, Small 13 (2017) 1603938.
[20] T. Sano, S. Tsutsui, K. Koike, T. Hirakawa, Y. Teramoto, N. Negishi, K. Takeuchi, Activation of graphitic carbon nitride (g-C_3N_4) by alkaline hydrothermal treatment for photocatalytic NO oxidation in gas phase, J. Mater. Chem. A 1 (2013) 6489–6496.
[21] H. Xu, J. Yan, X. She, L. Xu, J. Xia, Y. Xu, Y. Song, L. Huang, H. Li, Graphene-analogue carbon nitride: novel exfoliation synthesis and its application in photocatalysis and photoelectrochemical selective detection of trace amount of Cu^{2+}, Nanoscale 6 (2014) 1406–1415.
[22] M. Lima, P. Tavares, A. Silva, C. Silva, J. Faria, Selective photocatalytic oxidation of benzyl alcohol to benzaldehyde by using metal-loaded g-C_3N_4 photocatalysts, Catal. Today 287 (2017) 70–77.
[23] A. Jorge, D. Martin, M. Dhanoa, A. Rahman, N. Makwana, J. Tang, A. Sella, F. Corà, S. Firth, J. Darr, P. McMillan, H_2 and O_2 evolution from water half-splitting reactions by graphitic carbon nitride materials, J. Phys. Chem. C 117 (2013) 7178–7185.
[24] Z. Zhou, J. Wang, J. Yu, Y. Shen, Y. Li, A. Liu, S. Liu, Y. Zhang, Dissolution and liquid crystals phase of 2D polymeric carbon nitride, J. Am. Chem. Soc. 137 (2015) 2179–2182.
[25] W. Oh, V. Chang, Z. Hu, R. Goei, T. Lim, Enhancing the catalytic activity of g-C_3N_4 through Me doping (Me = Cu, Co and Fe) for selective sulfathiazole degradation via redox-based advanced oxidation process, Chem. Eng. J. 323 (2017) 260–269.
[26] L. Yang, J. Huang, L. Shi, L. Cao, Q. Yu, Y. Jie, J. Fei, H. Ouyang, J. Ye, A surface modification resultant thermally oxidized porous g-$C_3N_4$with enhanced photocatalytic hydrogen production, Appl. Catal. B–Environ. 204 (2017) 335–345.
[27] H. Li, B. Sun, L. Sui, D. Qian, M. Chen, Preparation of water-dispersible porous g-$C_3N_4$with improved photocatalytic activity by chemical oxidation, Phys. Chem. Chem. Phys. 17 (2015) 3309–3315.
[28] M. Solum, C. Mayne, A. Orendt, R. Pugmire, J. Adams, T. Fletcher, Characterization of macromolecular structure elements from a green river oil shale, I. Extracts, Energy Fuel 28 (2013) 453–465.
[29] V. Datsyuk, M. Kalyva, K. Papagelis, J. Parthenios, D. Tasis, A. Siokou, I. Kallitsis, C. Galiotis, Chemical oxidation of multiwalled carbon nanotubes, Carbon 46 (2008) 833–840.
[30] S. Guo, Y. Zhu, Y. Yan, Y. Min, J. Fan, Q. Xu, Holey structured graphitic carbon nitride thin sheets with edge oxygen doping via photo-Fenton reaction with enhanced photocatalytic activity, Appl. Catal. B–Environ. 185 (2016) 315–321.
[31] D. ark, K. Lakhi, K. Ramadass, M. Kim, S. Talapaneni, S. Joseph, U. Ravon, K. Bahily-Al, A. Vinu, Energy efficient synthesis of ordered mesoporous carbon nitrides with a high nitrogen content and enhanced CO_2 capture capacity, Chem. Eur. J. 23 (2017) 10753.
[32] P. Niu, L. Yin, Y. Yang, G. Liu, H. Cheng, Increasing the visible light absorption of graphitic carbon nitride (melon) photocatalysts by homogeneous self-modification with nitrogen vacancies, Adv. Mater. 26 (2014) 8046–8052.
[33] H. Gao, S. Yan, J. Wang, Y. Huang, P. Wang, Z. Li, Z. Zou, Towards efficient solar hydrogen production by intercalated carbon nitride photocatalyst, Phys. Chem. Chem. Phys. 15 (2013) 18077.
[34] J. Zhu, P. Xiao, H. Li, S. Carabineiro, ChemInform abstract: graphitic carbon nitride: synthesis, properties, and applications in catalysis, ACS Appl. Mater. Interfaces 6 (2014) 16449.
[35] Y. Wang, M. Bayazit, S. Moniz, Q. Ruan, C. Lau, N. Martsinovich, J. Tang, Linker-controlled polymeric photocatalyst for highly efficient hydrogen evolution from water, Energy Environ. Sci. 10 (2017) 1643–1651.
[36] G. Mane, S. Talapaneni, K. Lakhi, H. Ilbeygi, U. Ravon, K. Albahily, T. Mori, D. Park, A. Vinu, Highly ordered nitrogen-rich mesoporous carbon nitrides and their superior performance for sensing and photocatalytic hydrogen generation, Angew. Chem. Int. Ed. 56 (2017) 8481.
[37] M. Li, L. Zhang, X. Fan, Y. Zhou, M. Wu, J. Shi, Highly selective CO_2 photoreduction to CO over g-C_3N_4/Bi_2WO_6 composites under visible light, J. Mater. Chem. A 3 (2015) 5189–5196.
[38] X. Wang, K. Maeda, A. Thomas, K. Takanabe, G. Xin, J. Carlsson, K. Domen, M. Antonietti, A metal-free polymeric photocatalyst for hydrogen production from water under visible light, Nat. Mater. 8 (2009) 76–80.
[39] J. Shi, On the synergetic catalytic effect in heterogeneous nanocomposite catalysts, Chem. Rev. 113 (2013) 2139–2181.
[40] L. Li, P. Salvador, G. Rohrer, Photocatalysts with internal electric fields, Nanoscale 6 (2014) 24–42.
[41] M. Liu, X. Xue, S. Yu, X. Wang, X. Hu, H. Tian, H. Chen, W. Zheng, Improving photocatalytic performance from Bi_2WO_6@MoS_2/graphene hybrids via gradual charge transferred pathway, Sci. Rep. 7 (2017) 3637.
[42] J. Ran, G. Gao, F. Li, T. Ma, A. Du, S. Qiao, Ti_3C_2 MXene co-catalyst on metal sulfide photo-absorbers for enhanced visible-light photocatalytic hydrogen production, Nat. Commun. 8 (2017) 13907.